[Paper Number]

Space-Deployed Inflatable Dual-Reflector Antenna: Design and Prototype Measurements

Jesse H. Mills, Alan J. Fenn, Sean Crowley, Bakari Hassan, Frank C. Robey, Pierre Dufilie, Michael H. Hecht*
Massachusetts Institute of Technology, Lincoln Laboratory 244 Wood Street, Lexington, MA 02420, USA
*Massachusetts Institute of Technology, Haystack Observatory 99 Millstone Road, Westford, MA 01886, USA
(781)-981-2678

{jmills, ajf, robey, pierre.dufilie}@ll.mit.edu, mhecht@haystack.mit.edu
seanleocrowley@gmail.com, bakarihassan@cmu.edu

ABSTRACT

Large RF apertures have long proven to be a vexing challenge for small satellite/CubeSat platforms due to inherent mass and volume restrictions which has limited their use in SAR imaging, RF communications, and astronomy. Fixed apertures are fundamentally limited by the size of the platform itself so these restrictions drive the satellite designer to deployable apertures within which two primary classes exist: mechanical deployables and inflatable balloons. The primary trade between the two is packed volume and surface precision/accuracy per deployed aperture area. Inflatables offer significantly better packed volume than a mechanical deployable, but it is significantly harder to realize high precision surfaces. This paper details an axisymmetric array-fed confocal parabolic Gregorian reflector inflatable antenna system that has been designed, built, and characterized in the RF for potential space deployment from a small-sat payload. The system features three individual inflation chambers, a 2.4 meter primary reflector chamber, an independently adjustable 0.25 meter sub-reflector, and a 2.7 meter diameter torus that packs down to $\sim$1.25U, making use of this system feasible on many CubeSat platforms. The innovative implementation of the Gregorian design relaxes the fabrication tolerances required to achieve good RF performance. A novel approach for post-assembly correction of fabrication defects in the primary reflector has also been developed. Initial prototypes demonstrated approximately 38 dBi of gain with a $\sim 1^\circ$ beamwidth at 10 GHz. This represents an improvement in realized gain of greater than 13 dBi, 6 dB improvement in primary reflector surface efficiency, while also increasing reflector aperture diameter by a factor of 2.4 over recent literature. A path forward to improve the manufacturing design to achieve higher performance at X-band and enable Ku-band capability is also discussed as well as considerations for deployment and use in a space environment.

Keywords - Gregorian, reflector, antenna, array, inflatable antenna, deployable, apertures, CubeSats, small satellites.

INTRODUCTION

Reflector antennas with array feeds are of general interest for space applications requiring high gain, limited beam scanning, and low side lobes for communications and sensing applications. In the case of a space-deployable antenna, both low mass and low stowed volume are important goals, which might be achieved using an inflatable design as depicted as an artists concept in Figure 1. In this study, an axisymmetric Gregorian antenna system design with confocal paraboloids was desired, which could allow easier fabrication compared to an offset Gregorian design.[1–4] Ray tracing shows that the confocal paraboloid geometry provides alignment of the primary and secondary reflectors, and a phased array feed provides additional shape compensation and limited electronic scanning making it a good choice for implementation as an inflatable antenna.[4] Thin-film materials with and without electrically conducting coatings can be considered for designing an inflatable space-deployable antenna.[5–8] A previous study analyzed a Ku-band axisymmetric Gregorian antenna system with a phased array feed for limited electronic beam steering.[9,10] For simulation purposes, an ideal planar array source feeding the Gregorian sub-reflector is assumed in the current study. When a large focal magnification is used, the blockage of the main beam by the sub-reflector can be relatively small, which enables high gain and low side lobes. Future deep space missions may require large deployable aperture antennas with electronic scanning to perform radio navigation by measuring time-of-arrival and microwave Doppler shift signatures of millisecond pulsars,[11] and the antenna may also be used for communications – antenna diameters on the order of 1 to 10 meters are of interest.

DISTRIBUTION STATEMENT A. Approved for public release. Distribution is unlimited. This material is based upon work supported by the United States Air Force under Air Force Contract No. FA8702-15-D-0001. Any opinions, findings, conclusions or recommendations expressed in this material are those of the author(s) and do not necessarily reflect the views of the United States Air Force.

The design and methods covered in this paper have four key contributions to inflatable antenna development:

- An inflatable dual-reflector antenna with a 2.4 meter diameter primary and empirical measurements exceeding the state of the art gain at X-band by over 13 dBi (Babuscia et al. 1m diameter reflector)[12]
- An inflatable dual-reflector antenna with empirical X-band measurements demonstrating both a primary reflector surface efficiency improvement exceeding 6 dB and a 2.4x increase in primary reflector aperture diameter over Babuscia et al[12]
- A novel three-chamber design that enables antenna alignment and wrinkle removal both on the ground after assembly and in orbit
- A flexible design approach enabling high-performing inflatable structures by emphasizing post-assembly design adjustability rather than a traditional approach focused on design precision

This paper is organized as follows. In the next section, the design of an array-fed Gregorian reflector system with a 2.4 meter diameter main reflector is given. The antenna is analyzed and optimized at Ku-band using numerical simulations with the multilevel fast multipole method (MLFMM). Simulated results at Ku-band are then shown in the following section. Afterwards, a prototype axisymmetric Gregorian antenna with an X-band feed is described, followed by prototype measurements and simulated results along with recommendations for further improvements. Finally, a summary of the design, fabrication, results, and contributions is provided.

NUMERICAL SIMULATION & MODELING

A Gregorian confocal reflector system has been designed, analyzed, and optimized using numerical simulations conducted with the FEKO (`www.feko.info`) software MLFMM solver shown in Figure 2. The design consists of a 2.4 meter diameter primary parabolic reflector with a 0.9 meter focal distance, 0.25 meter diameter parabolic sub-reflector with a focal distance of 0.08 meter, and a 0.2 meter planar array. A design summary is provided in Table1. Key assumptions driving our numerical analysis were that the primary and secondary reflectors were perfect electric conductors with ideal parabolic shape. Optimization was performed at 16 GHz (1.875 cm) as a grid search with the sub-reflector diameter and sub-reflector focal distance as the search parameters. The objective of the grid search optimization program was achieving optimal peak directivity at boresight.

For example, consider Ku-band operation at 16 GHz. In this case, the simulated array feed shown in Figure 3 is assumed to be an ideal 20 cm diameter circular aperture source with 140 linearly polarized elements spaced 1.5 cm (0.8λ) apart on a square grid. The feed array is adjacent to the satellite body, and is spaced 3 cm from the vertex of the primary reflector. The feed array half-power beamwidth is 5.5° at 16 GHz, and the angle from the center of the array to the edge of the sub-reflector is $\pm 5^\circ$, so the sub-reflector will be illuminated with minimal spillover losses. At X-band (10 GHz), with the same reflector optics and same size feed diameter, the sub-reflector spillover would be higher and the side lobes would be elevated. The magnification factor for this system is the ratio of the primary to sub-reflector focal distances which is 11.25. Note that with the dual reflector optics shown in Figure 1,the antenna radiation beam is pointed away from the satellite body.

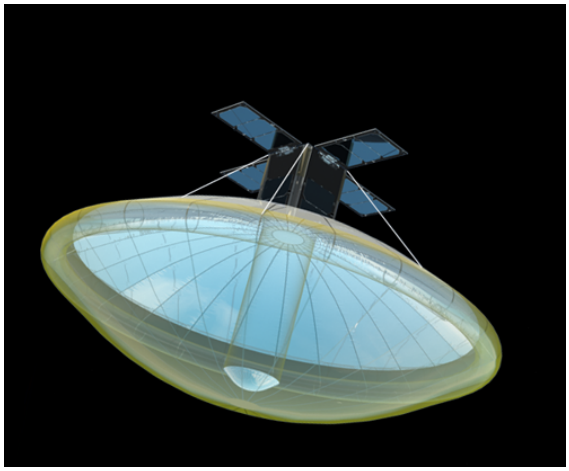

Figure 1. Artist's concept for an inflatable axisymmetric dual-reflector antenna deployed from a satellite.

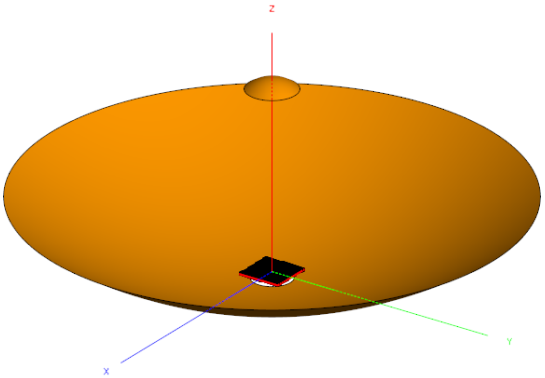

Figure 2. Electromagnetic model for a Ku-band axisymmetric Gregorian antenna with confocal paraboloids and planar array feed.

Table 1. Key Antenna Design Dimensions

Measurement	Primary Reflector	Secondary Reflector	Planar Array
Diameter (meters)	2.4	0.25	0.2
Focal Distance (meters)	0.9	0.08	N/A
f/D Ratio	0.375	0.32	N/A

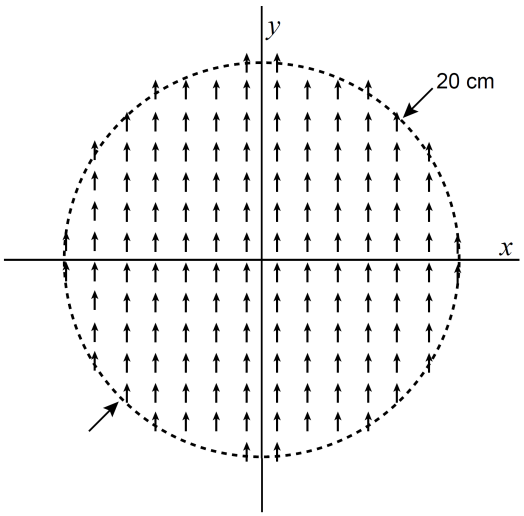

Figure 3. Simulation model of circular feed array with uniform amplitude illumination.

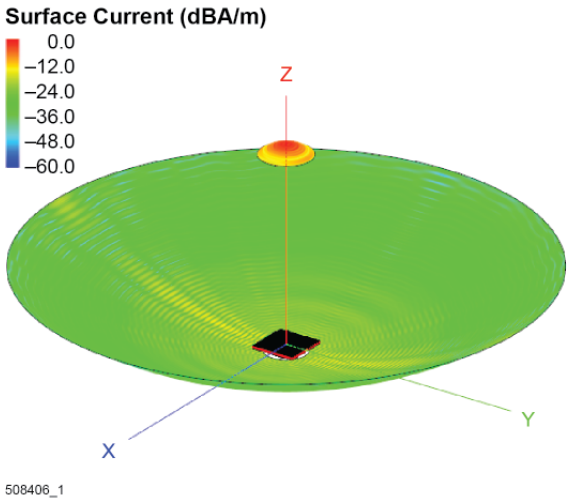

Figure 4. Simulated surface currents at 16 GHz.

KU-BAND SIMULATED RESULTS

The MLFMM simulated surface currents in dBA/m on the primary and secondary reflectors are shown in Figure 4. Direct illumination of the 2.4 meter diameter primary reflector from the near-field side lobes of the array feed is observed. The simulated near-field radiation pattern (total field) is shown in Figure 5. The simulated E-plane and H-plane directivity patterns at 16 GHz are shown in Figure 6. The simulated radiation pattern characteristics are as follows: directivity is 49.4 dBi, half-power beamwidth is 0.52 , and first sidelobe level is 28.5 dB. For a 2.4 meter diameter aperture with 100% efficiency, the peak directivity at 16 GHz is 52 dBi, so the simulated aperture efficiency of this antenna design is 55%.

The above FEKO simulated results in Figure 6 assume ideal primary and secondary reflector surfaces. To provide an estimate of the peak antenna gain versus RMS surface errors for the primary reflector with an ideal sub-reflector, simulated results using GRASP software are shown for 10 GHz and 16 GHz in Figure 7. For example, primary reflector surface RMS errors of 0.033 inches (0.838 mm) spaced 4.7 inches (11.94 mm) apart yields 1 dB of peak gain reduction at 16 GHz.

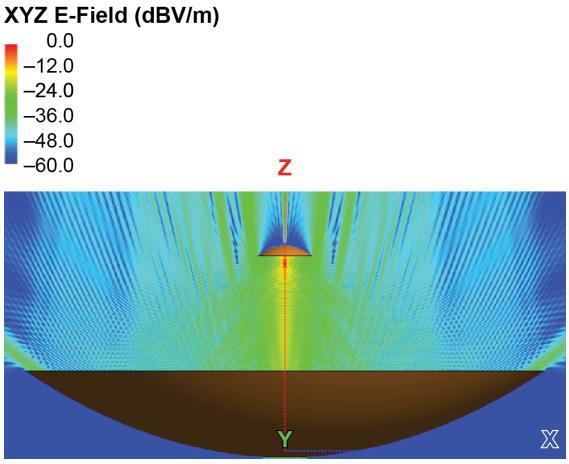

Figure 5. Simulated surface currents at 16 GHz.

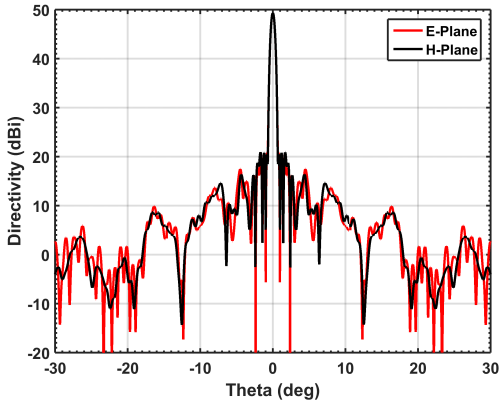

Figure 6. Simulated surface currents at 16 GHz.

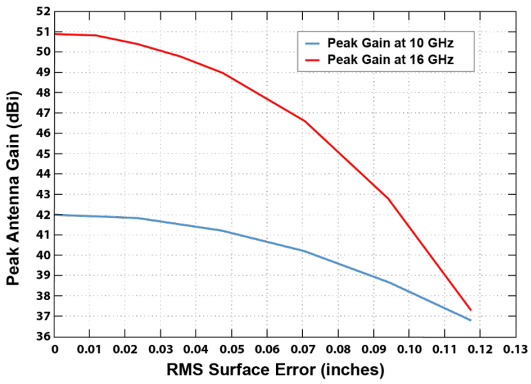

Figure 7. Simulated peak antenna gain versus RMS surface errors on the primary reflector with an ideal sub-reflector at 10 GHz and 16 GHz.

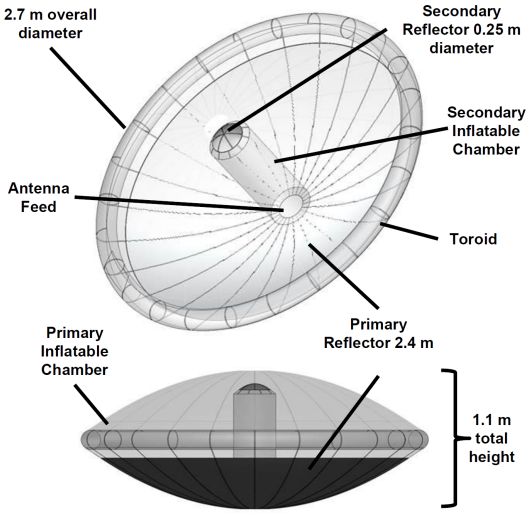

Figure 8. Prototype inflatable Gregorian reflector antenna design.

MECHANICAL DESIGN

For this particular prototype inflatable antenna, the dual-reflector Gregorian antenna design consists of a 2.4 meter diameter primary reflector and a 0.25 meter secondary reflector that form a pair of confocal paraboloids as shown in Figure 8.

As shown in Figure 8, the feed is an array antenna or other type of antenna aperture at the base of the primary reflector and directly illuminates the secondary reflector, which in turn illuminates the primary. The implementation of the dual reflector Gregorian antenna is effected by three separate inflatables, a primary chamber to inflate the main reflector and contains a canopy that is symmetric to the main reflector, a cylindrical secondary chamber to inflate the sub-reflector which also contains the RF feed, and a toroid to force the parabolic primary chamber to a parabolic shape. Without a toroid in the design as shown in Figure 8 the parabolic primary shape would become quasi-spherical regardless of fabrication precision upon inflation.

The process for designing the inflatable antenna prototype began with building a 3D model in SolidWorks of the prototype design with each inflation chamber designed as its own subassembly. Different surfaces within the design are segmented into individual gores that are treated as individual components. The surfacing add-on in SolidWorks is then used to project each of these 3D gores to a 2D flat surface. This 2D flat surface is the basis of the gore template design used for cutting gores from sheets of polymeric material an example of which is shown in Figure 9. These gores are joined together by pressure sensitive adhesive (PSA) tape over a mandrel that mimics, to within machining tolerances, the desired curvature of the surface. Taping gores together over a mandrel designed in this way forces the

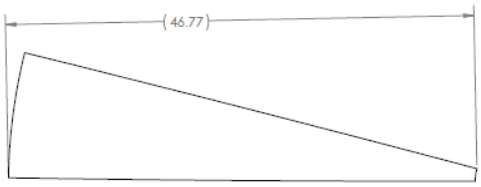

Figure 9. Primary reflector and canopy gore template. Mandrel is made of low-cost 0.125 inches 6061 aluminum sheet metal using low-cost water jet fabrication.

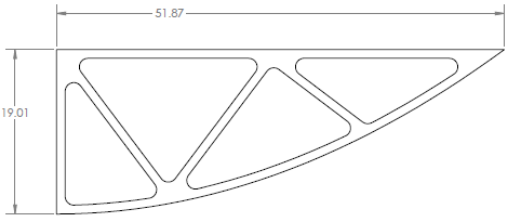

Figure 10. Primary reflector and canopy taping mandrel. Mandrel is 1 inch thick and made of low-cost acrylic using low-cost water jet fabrication.

2D flat gore shapes to adopt the desired 3D curvature at the tape seam and areas between adjacent tape seams upon inflation. The mandrels are designed by taking the desired surface shape and adding structure to the basic shape such that it can be easily mounted to an ordinary work bench as shown in Figure 10. In this case the shapes of interest are parabolic (primary reflector, primary canopy, secondary reflector) and cylindrical (secondary chamber, toroid) but the technique extends equally to spherical, conical, and other curvatures such as elliptical, hyperbolic, etc. In both cases, these mandrels and gore templates are made from low-cost, readily available materials and are designed such that low-cost fabrication techniques such as a water jet can be used to fabricate them.

Fully 3D taping mandrels were required in two places in the design to ensure adequate surface accuracy. The secondary reflector alignment atop its cylindrical inflation chamber was critical as errors here could not easily be adjusted low-costpost-assembly. For this part of the assembly a taping mandrel was grown via fused deposition modeling (FDM) that contained the secondary reflector surface shape out to the transition to its cylindrical inflatable chamber mount as well as alignment and keying features to ensure proper alignment of the secondary reflector to its cylindrical mount. This minimizes unresolvable tip/tilt errors in the primary relative to the feed as well as minimizes wrinkling at the secondary surface to its cylindrical mount interface. Also, RF transparent extension pieces were added to the pri-

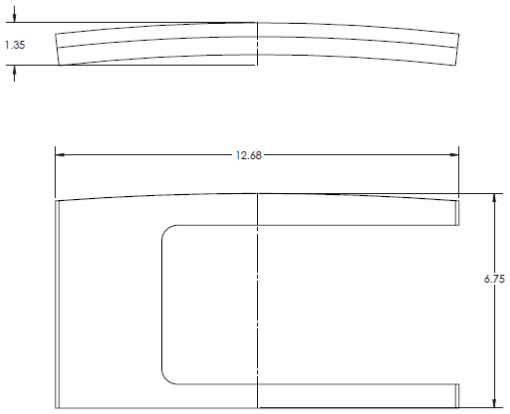

Figure 11. Primary RF extension taping mandrel design exhibiting curvature in two axes.

mary reflector and canopy to mitigate surface wrinkling that is expected at the primary/canopy to toroid interface. This tape seam has curvature in two directions, therefore a mandrel was designed and fabricated that reflected this curvature. The design for this mandrel is shown in Figure 11.

A key aspect in the design of an inflatable is balancing the number of gores necessary to replicate the 3D shape with high fidelity and the stowed volume to packing factor ratio. As described above, the gores taped together over mandrels that replicate the desired curvature will result in a highly accurate replication of the desired curvature at the tape seam. However, depending on the material stiffness and the distance between tape seams, itself a function of gore count and characteristic diameter of the surface being created, significant flattening of the surface between tape seams can be observed. Higher number of gores will lead to better surface quality; however, significant numbers of tape seams will impact packing factor and other design aspects such as leak rate, overall strength and even reliability (higher chance of introducing a fatal defect). Fewer gores will mitigate concerns with leak rate, overall strength and reliability but will result in much more significant flattening that will result in reduced performance that is harder to recover with low-cost post-assembly correction processes described later in this paper. 2 summarizes the basic design, gore counts, materials selection, and inflation pressure/stress of each chamber.

Materials Selection

In ground-based testing, the toroid is pressurized to 3.0 psig, and is constructed out of 24 individual sections each comprised of two individual gores. The toroid has an outer diameter of 2.7 m, a minor diameter of 15.24 cm (6 inch), and was made using 0.0508 mm (0.002 inch) thick Kapton film. Each joint is taped

Table 2. Material selection and detailed design aspects for three distinct inflatable chambers

	Primary	Secondary	Toroid
Material	Half Melinex 377 0.0254 mm thick Half Melinex 377 0.0254 mm thick With 30 nm VDA	Part Melinex 377 0.0254 mm thick Part Melinex 377 0.0254 mm thick With 30 nm VDA	0.0508 mm thick Kapton
Tape	2.54 cm wide Silicon PSA Kapton HN Carrier .00762 mm thick	1.27 cm wide Silicon PSA Kapton HN Carrier .00762 mm thick	2.54 cm wide Silicon PSA Kapton HN Carrier .0254 mm thick
Construction	2 Parts 24 Sections Each 2 Gores/Section	Reflector: 10 Sections Telescoping Adjustment: 2 Gores	24 Sections 2 Gores/Section
Size	2.7 m Outer Dia 1.1 m in Height	.25 m Dia 0.9 m Length	2.7 m Outer Dia 0.1524 m Minor Dia
Pressure (psig)	0.05	0.4	3.0
Skin Stress (psi)	2657.5	1968.5	4643.1

together using a 2.54 cm wide silicone PSA tape with a 0.0254 mm (0.001 inch) thick Kapton HN carrier. The main function of the toroid is to maintain the shape of the primary reflector. The primary inflatable section is composed of a primary reflector and a symmetric canopy that is taped to the torus with the same tape used in the toroid assembly. The primary and canopy sections are constructed out of 24 sections each taped together with a 2.54 cm (1 inch) wide silicone PSA tape with a 0.00762 mm (0.0003 inch) Kapton HN carrier. The sections of the primary and canopy are made from combinations of bare 0.0254 mm (0.001 inch) thick Melinex 377 (Polyester) and 0.0254 mm (0.001 inch) thick Melinex 377 (polyester) film coated with 30 nm of vapor deposited aluminum (VDA).

A Flexible Design Approach

Given the imprecise nature of inflatable construction as compared to traditional fixed aperture designs, post-fabrication adjustability is critical to realizing a functional inflatable antenna. While the multi-chamber design of this antenna complicates fabrication, it facilitates design concepts that make this design robust to fabrication defects and flexible enough to accommodate post-fabrication and post-deployment adjustments, and tuned inflation pressures designed to minimize surface wrinkling. Even fixed aperture designs carry some of these features to account for machining and assembly tolerances, yet the literature regarding inflatable antenna design and development does not embrace these approaches. Finally, a design/build/characterize prototyping approach was embraced as opposed to detailed mechanical modeling of the design. This approach also stems from the fact that the imprecise nature of inflatable fabrication is difficult to account for in models and therefore makes an analysis/design/build cycle lengthier process owing to misleading model results that can take a long time to produce.[13,14] Given that inflatables of this kind are typically hand built, variability within a given antenna and across different antennae built at different times with different technicians and engineers should be expected. These are issues that are very diffi-

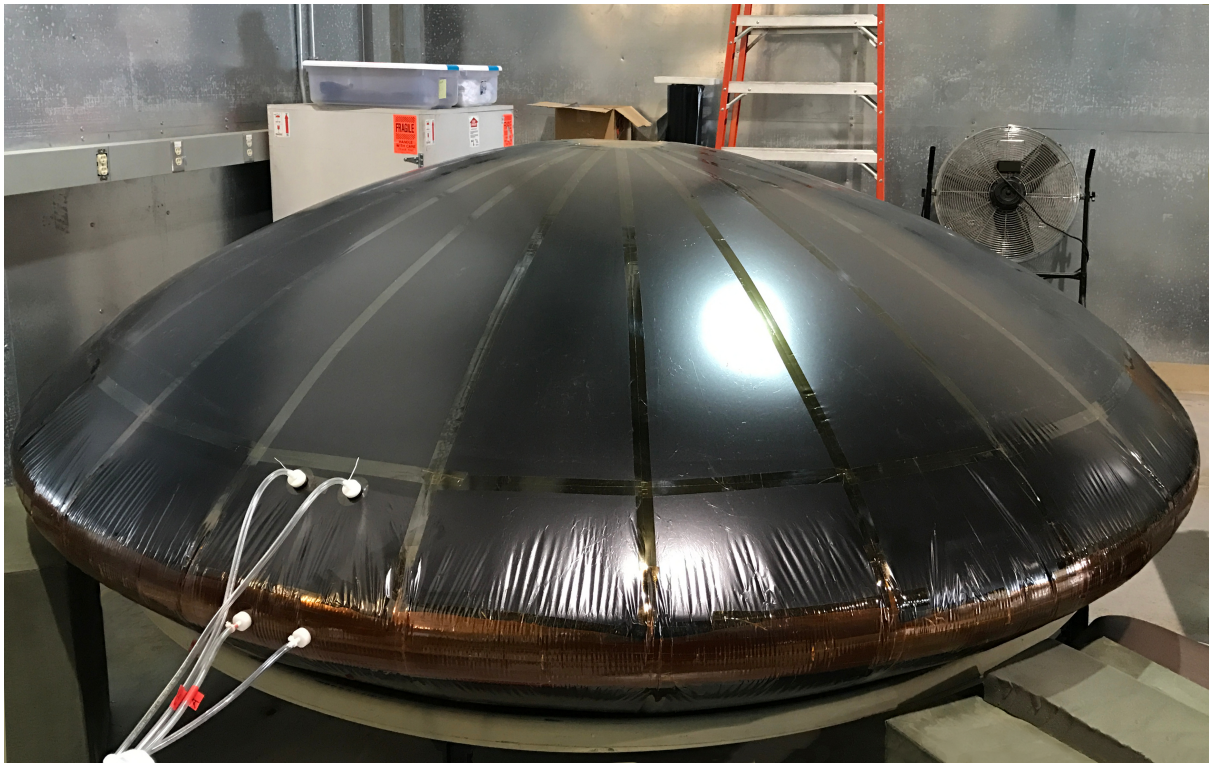

Figure 12. Prototype antenna shown after undergoing assembly, inspection, and adjustment with the exterior side of the canopy visible on top and the amber-colored toroid visible along the perimeter.

cult to properly capture in any conceivable mechanical model. Thus the emphasis in this effort was focused on prototyping and characterization along with features placed in the design and fabrication to account for this inevitable variability to produce an antenna that can provide consistent end product performance regardless of who is building it. The fixturing required to build an inflatable with the methods described above is straightforward and inexpensive, so multiple prototyping cycles are quick and cost effective.

Eliminating Wrinkles

As described above, the assembly of the antenna includes integration of the primary reflector to the torus. At this interface, significant wrinkling is expected (and has been observed by other investigators[7, 8, 15]) so the design included a 30 cm section of RF transparent material (Melinex 377). The section was sized such that when the primary and torus were inflated to their design pressures the wrinkling in the primary surface would be damped out, implying the stress field in the primary had become largely uniform, resulting in no large scale distortion of the actual reflector surface. While this design feature adds slightly to the overall packed volume of the inflatable antenna, it is a very small amount making the trade between packed volume and reflector surface quality well worth it. The same approach was taken with the secondary reflector and its interface to the cylindrical secondary inflation chamber. The canopy in the primary inflatable was designed to be symmetric with respect to the primary reflector surface to balance the loads on the torus due to primary inflation forces to within the inflatables fabrication precision.

The pressures selected for each inflatable were chosen to minimize wrinkles in the RF reflective surfaces and maximize the observed performance. Pressures above those specified in 2 produced no noticeable improvements in gain or side lobes. The stresses in 2 that result from these pressures are 15-50% of the yield stress of the Melinex 377 and 0.2% of the Kapton HN. While different materials selection may modify the precise optimized pressure for a given inflation chamber of a given design, it appears a target stress of at least 15% of the yield stress of the material is desirable. Determination of the optimal pressure of a given design and set of materials should be done through prototyping and characterization.

Post-Assembly Fine Adjustment of the Primary Reflector

A novel process for removing post-fabrication and assembly surface errors was developed and could be described as reverse thermoforming is shown in Figure 13. In typical thermoforming processes of thin film materials, compression at high pressure and temperature is used that requires special thermoformable materials.

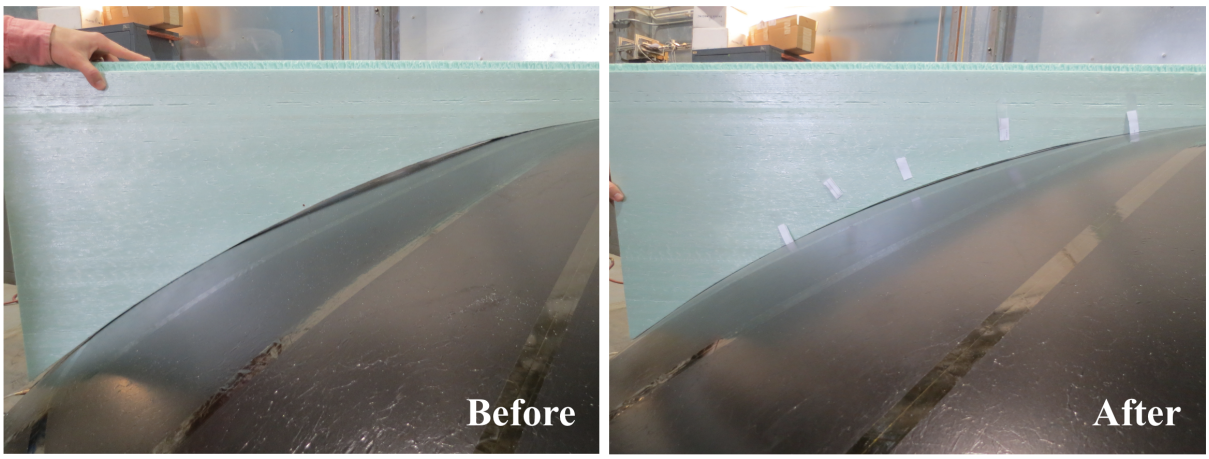

Figure 13. Left: Newly assembled and inflated reflector surface is a parabolic, mismatching the parabolic template. Right: Parabolic reflector achieved through thermoforming.

The process forces the material to take the shape of a precision machined mandrel. This process has several drawbacks; first, it can cause damage to the films, even if the film is designed for it, second, the restriction to specially defined films that can tolerate a compression thermoforming process limit design trade space for other important considerations such as overall structural strength and elasticity, optical properties, adhesion properties and others, finally, forming a thin film membrane over a several meter diameter surface will require costly, exquisitely machined and assembled mandrels to ensure the applied compression and temperature are applied uniformly. In the reverse thermoforming process the inflation stress, which is naturally a very uniform tensile stress throughout the material, is used along with local application of moderate heat. A reference mandrel was developed that is essentially the mirror image of the taping mandrels described previously. The surface is heated and allowed to creep viscoelastically under load until any gap with the reference mandrel is closed. Because the expansion of the material under load and temperature contains both elastic and plastic components this heating process is repeated cyclically until the desired shape is achieved. While the deformation of the material, in principle, causes some thinning of the film to occur, no degradation of mechanical strength was observed nor was there any degradation of the VDA coating observed visually or in RF characterization. The major benefits of this approach are low-cost mandrels, localized application of moderate amounts of heat, and effective for any thin film material as all thin film polymeric materials exhibit viscoelastic creep to varying degrees. For this work, a Conair ProStyle 1500 hair dryer was found to be ideal for reshaping the primary surface and did not exceed $50°C$ and a simple form was made out of ordinary solid Styrofoam building insulation. Figure 14 shows the 2.4 meter antenna prototype being prepared for anechoic chamber testing.

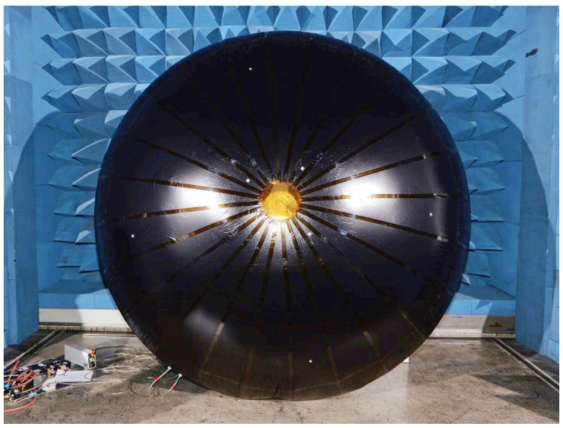

Figure 14. Preparing the 2.4 meter antenna prototype for RF characterization in the compact range. The tip of the secondary chamber is visible through the amber pole cap.

Post-Assembly Alignment

The secondary inflation chamber was designed to be integral with the RF feed and taped into the vertex of the primary reflector surface. This allows the primary reflector to be independently positioned relative to the secondary. It also enables precision alignment through a closed loop pitch/yaw winching/lanyard mechanism not only in the RF characterization chamber, but also in flight. A simple positioning system controlled with on board RF diagnostics enables completely self-contained post-deployment alignment and calibration. The shape and internal pressure of the secondary inflatable also allow a high degree of position repeatability between inflations, providing a high level of confidence performance measured on the ground will be repeatable in orbit.

The secondary inflation chamber also contains a telescoping feature that allows for changing the height of

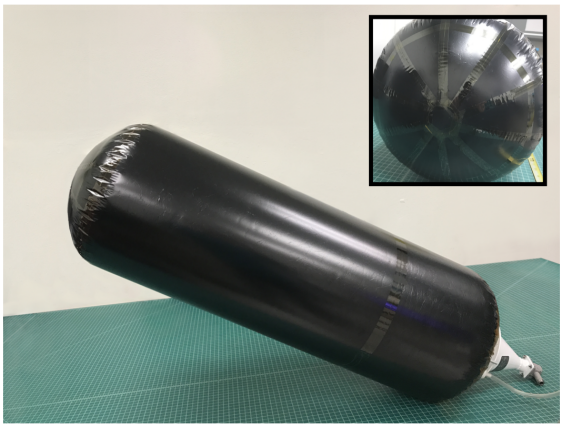

Figure 15. Secondary chamber with feed horn attached on the right side. Top right: a close-up of the external convex side and ten gores composing the secondary parabolic reflector.

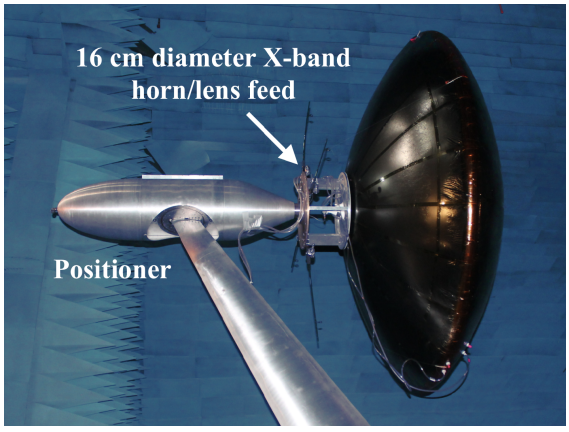

Figure 16. Inflated Gregorian reflector antenna during compact range measurements with a horn-lens feed at X-band.

the secondary reflector relative to the primary reflector to ensure that these two surfaces are truly confocal. Given that the secondary inflatable contains the RF feed and is largely independent of the primary, removal of this assembly and adjustment of its height based on characterization data is straightforward and quick. Typically, adjustments could be made to the secondary reflector position, and testing could resume within a day.

On-Orbit Inflation & Sustainment

The inflation of this system in space would be a three-step process: torus, primary, and finally the secondary chamber. Achieving the particular pressures for a given design would be affected by three individual containers of a liquid, such as water or propylene glycol mixture, heated to a prescribed temperature will produce a pressure based on its vapor pressure curve. Vapor pressure for aqueous propylene glycol as a function of temperature is shown in Figure 17 with potential design points detailed in Table 3. The heat for this kind of inflation mechanism can be implemented via ordinary spacecraft heater and control circuits. However, realistic operational lifetimes of an inflatable antenna system in space are likely to run longer than 6 months at the least and natural leak paths and those created by micrometeoroid interactions will make long-term pressurization by liquid (gas, sublimating powder as well) unrealistic. UV curable resins have been studied for this application for some time[16] and demonstrated in ground testing of inflatable antenna systems.[15] Application of a UV curable resin will minimize the SWaP and complexity of the inflation system by requiring it to be functional for a period of time on the order of a few hours to a few days. As of now the deployment and rigidization concepts have not yet been prototyped or tested.

Table 3. Inflation chamber temperatures necessary to achieve functional pressure levels for aqueous propylene glycol of varying mass percentages

Aqueous Propylene Glycol Mass Percentage	Primary (0.05 psia)	Secondary (0.4 psia)	Toroid (3.0 psia)
0	N/A	$22°C$	$57°C$
40	N/A	$24°C$	$60°C$
60	N/A	$28°C$	$65°C$
80	$3°C$	$33°C$	$77°C$
98	$35°C$	$60°C$	$115°C$
100	$60°C$	$96°C$	$137°C$

X-BAND CHARACTERIZATION RESULTS

Empirical measurements were made in the MIT Lincoln Laboratory compact range.[11,18] The inflated system is shown under test at this facility in Figure 16. A surrogate antenna (Flann Microwave, Horn-Lens Antenna, Model 16810-FA, 8.4 to 11.15 GHz, 15 cm diameter (`www.flann.com`)) was used in lieu of an array for X-band measurements. To help counter the effects of gravity-induced sag, four nonconductive lanyards were used for yaw-pitch control to position the primary relative to the secondary without distorting the primary reflector or interfering with the antenna beam pattern.

The measured realized E-plane and H-plane gain patterns of the surrogate horn-lens feed alone at 10 GHz are shown in Figure 18. The measured peak realized gain of this feed antenna is 22.1 dBi. When the measured H-plane directivity is compared with numerical simulations assuming ideal surfaces, there is a clear main lobe with the measured peak directivity is 37.6 dBi, which is 3.8 dBi lower than the simulated ideal value of 41.4 dBi as shown in Figure 19. In the simulation, ideal main reflector and sub-reflector surfaces and alignment were assumed.

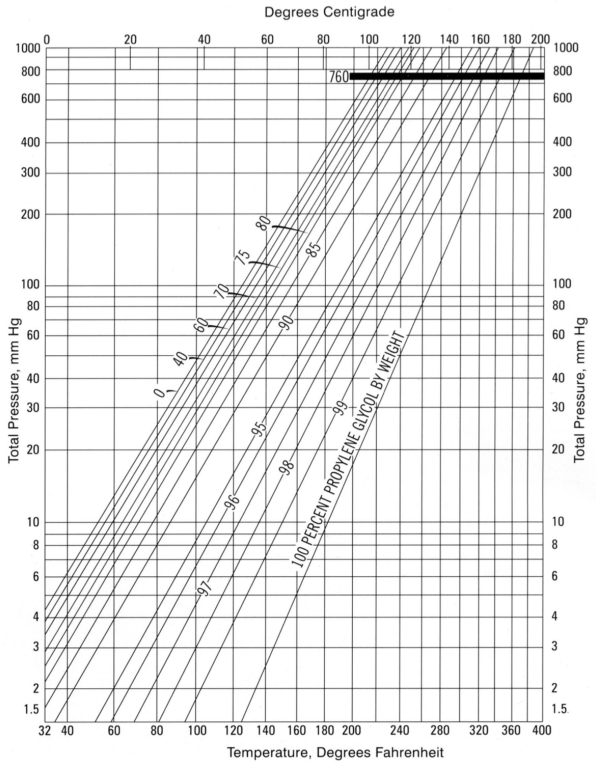

Figure 17. The designer can choose a water-glycol mixture percentage and a temperature to reach suitable internal pressures. Figure adapted from.[17]

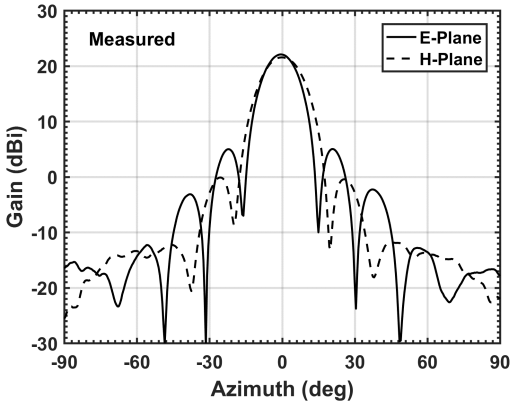

Figure 18. Measured E-plane and H-plane realized gain patterns for the horn-lens feed antenna alone at 10 GHz.

To investigate the sources of gain loss in the prototype antenna, a Metris MV220 3D laser radar was used to characterize the as-built geometry of the primary and secondary surfaces. These measured surfaces were then imported into the EM model to characterize their performance against the ideal surfaces with ideal alignment. The secondary surface showed very little noticeable gain loss when the as-built surface was modeled with an ideal primary reflector with ideal alignment indicating that the design and fabrication process for the secondary inflatable chamber is already sufficient.

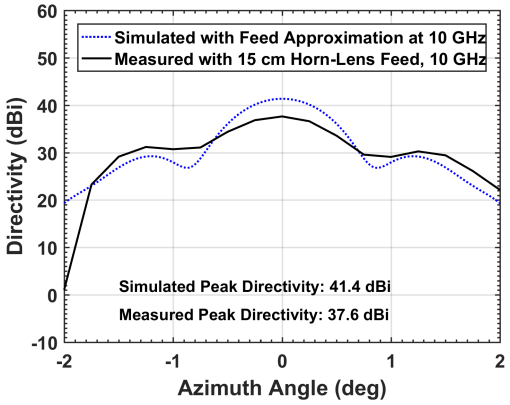

Figure 19. Measured directivity pattern of the inflated Gregorian reflector system at X-band compared with the simulated directivity pattern with ideal parabolic surfaces.

The primary surface, when modeled with an ideal subreflector and with ideal alignments, showed degradation of peak gain of similar magnitude to what was measured in the chamber as well as the overall antenna pattern. Figure 20 shows the finite element model generated from the 3D laser scan, and Figure 21 shows a comparison of predicted results using this model against the actual measurements on the same surface from the RF characterization range. There is good agreement between RF measurements and RF modeling derived from mechanical measurements of the same surface. Additionally, defects exclusive to the primary surface largely explain the measured gain and antenna beam pattern discrepancies. Both of these factors considered, this strongly indicates that the secondary fabrication, secondary adjustment, and secondary to primary alignment techniques developed and described in this paper were successful and sufficient. Remaining errors that result in degradation of gain and non-ideal antenna patterns are largely associated with the accuracy of the primary surface itself. The analysis discussed in a previous section and shown in Figure 7 suggests that the RMS surface error in the primary reflector is approximately 0.125 inches.

Recommended Design Improvements

Several improvements in the design and fabrication design have been identified that will result in improved performance. First, a circumferential seam in the primary and canopy at approximately the mid span between the sub-reflector interface and RF transparent panel interface at the outer edge would significantly educe the flattening effect of the reflective surface near the mid span of these gores. The flattening of these gores is visible Figure 13 which generally require thermoforming to remove. The result would be improved initial precision and accuracy of the reflective surface

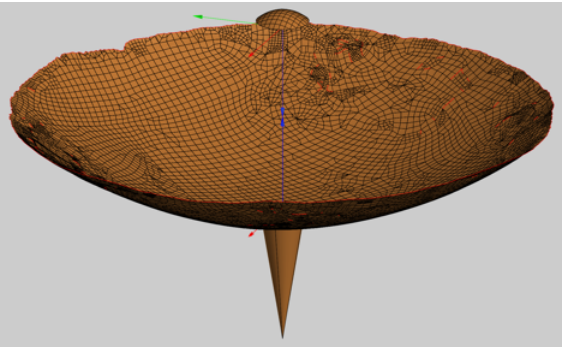

Figure 20. Finite element model of as-built prototype primary reflector surface as measure with a 3D laser radar

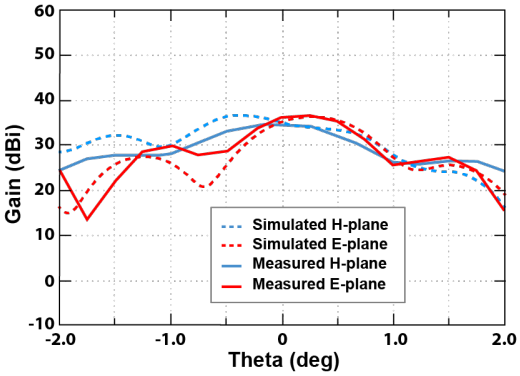

Figure 21. Electromagnetic simulation of 3D laser scanned primary surface vs. RF chamber measurements at 10 GHz of the same surface.

which would make adjustments implemented by the reverse thermoforming process more effective.

Second, the fixturing used to integrate the primary reflector and canopy to the torus was fairly crude and required a lot of judgement/visual estimation. The reverse thermoforming process also employed fairly primitive fixturing consisting of a hand cut reverse mandrel and an ordinary hair dryer with the process being implemented by hand. In both of these cases, it is easy to envision fixtures that will improve the precision and accuracy of the initial assembly as well as make the reverse thermoforming process low-cost post-assembly even more effective.

Finally, improvements in performance might also be possible with the use of a calibrated phased array feed to correct for residual surface distortions and alignment of the main reflector and sub-reflector as part of an in-flight calibration process.[19] The improvements, when considered together, should result in antenna performance that is within 1 dB of the ideal model predictions via a fabrication process that could be replicated by other organizations.

SUMMARY

An axisymmetric Gregorian dual-reflector antenna system with confocal paraboloids and a planar array feed has been explored for a possible space-deployed inflatable antenna. Optimization at Ku-band using the multilevel fast multipole method indicates high gain and low side lobes can be achieved for this antenna design. A three-chamber prototype inflated Gregorian antenna structure with a surrogate horn-lens feed has been fabricated and measured at X-band. Emphasis was placed on a prototyping/characterization approach with design and fabrication design approaches that allow for adjustment of surfaces and alignments through fabrication, ground characterization, and in-flight commissioning and calibration. This emphasis is critical to realizing a functional inflatable antenna for use in space applications and is based in acknowledgment of the imprecise and somewhat unpredictable nature of inflatables. The process developed in this work accounts for this and should result in a product with predictable performance from antenna to antenna regardless of who is building it. Results from this initial prototype show good performance at X band, exceeding the current state of the art in gain and directivity. With the design and fabrication design improvements highlighted in this paper, performance within 1 dB of ideal at X-Ku band should be realizable. Other frequencies might be possible for future space-deployed antenna systems using this design approach as well as apertures up to 10 meters.

Acknowledgments

Technical discussions with Jason R. Franz, Pamela R. Evans, H. David Goldfein, Robert G. Atkins, Jeffrey S. Herd, Dennis A. Burianek, and James Finnell are sincerely appreciated. The antenna measurements were performed by David M. Bruno, Paul A. Theophelakes, and Richard J. Cotillo. Casey Reed and Allison Loftin provided graphic art support.

References

1 Wilson, C., "Electronically Steerable Field Reflector Techniques." Tech. rep., Airborne Instruments Lab Deer Park NY, 1965.

2 Fitzgerald, W. D., "Limited electronic scanning with an offset-feed near-field Gregorian system," Tech. rep., Massachusetts Inst. of Tech Lexington Lincoln Lab, 1971.

3 Martinez-Lorenzo, J. A., Garcia-Pino, A., Gonzalez-Valdes, B., and Rappaport, C. M., "Zooming and scanning Gregorian confocal dual reflector antennas," *IEEE Transactions on antennas and propagation*, Vol. 56, No. 9, 2008, pp. 2910–2919.

4 Fenn, A. and Richardson, R., "Analysis of an adaptive two-reflector phased-array fed system," *1980 Antennas and Propagation Society International Symposium*, Vol. 18, IEEE, 1980, pp. 134–137.

5 Freeland, R., Bilyeu, G., and Veal, G., "Development of flight hardware for a large, inflatable-deployable antenna experiment," *Acta Astronautica*, Vol. 38, No. 4-8, 1996, pp. 251–260.

6 Xu, Y. and Guan, F.-l., "Structure design and mechanical measurement of inflatable antenna," *Acta Astronautica*, Vol. 76, 2012, pp. 13–25.

7 Babuscia, A., Van de Loo, M., Wei, Q. J., Pan, S., Mohan, S., and Seager, S., "Inflatable antenna for CubeSat: fabrication, deployment and results of experimental tests," *2014 IEEE Aerospace Conference*, IEEE, 2014, pp. 1–12.

8 Babuscia, A., Choi, T., Lee, C., and Cheung, K.-M., "Inflatable antennas and arrays for interplanetary communication using CubeSats and smallsats," *2015 IEEE Aerospace Conference*, IEEE, 2015, pp. 1–9.

9 Fenn, A. J., Mills, J. H., Robey, F. C., Dufilie, P., and Hecht, M. H., "Axisymmetric Gregorian Reflector System for a Space-Deployed Inflatable Antenna: Simulations and Measurements," *Submitted to 2019 IEEE International Symposium on Phased Array Systems and Technology*, IEEE, 2019, pp. 1–4.

10 Fenn, A. J., *Electromagnetics and Antenna Technology*, Artech House, 2017.

11 Jessner, A. and MPIfR, B., "Technical requirements for autonomous space craft navigation using radio pulsars," Proceedings of the 593rd WE-Heraeus Seminar on Autonomous Spacecraft , 2015.

12 Babuscia, A., Choi, T., Sauder, J., Chandra, A., and Thangavelautham, J., "Inflatable antenna for CubeSats: Development of the X-band prototype," *2016 IEEE Aerospace Conference*, IEEE, 2016, pp. 1–11.

13 Greschik, G., Mikulas, M., Palisoc, A., Cassapakis, C., and Veal, G., "Approximating paraboloids with axisymmetric pressurized membranes," *39th AIAA/ASME/ASCE/AHS/ASC Structures, Structural Dynamics, and Materials Conference and Exhibit*, 1998, p. 2102.

14 Sreekantamurthy, T., Gaspar, J., Mann, T., Behun, V., Pearson, J., and Scarborough, S., "Nonlinear structural analysis methodology and dynamics scaling of inflatable parabolic reflector antenna concepts," *48th AIAA/ASME/ASCE/AHS/ASC Structures, Structural Dynamics, and Materials Conference*, 2007, p. 1834.

15 Babuscia, A., Sauder, J., Chandra, A., Thangavelautham, J., Feruglio, L., and Bienert, N., "Inflatable antenna for CubeSat: A new spherical design for increased X-band gain," *2017 IEEE Aerospace Conference*, IEEE, 2017, pp. 1–10.

16 Hoyt, A. E., Harrah, L. A., Sprouse, M. R., Allred, R. E., McElroy, P. M., Scarborough, S. E., and Cadogan, D. P., "Light curing resins for rigidizing inflatable space structures," *Proceedings of 49th International SAMPE Symposium and Exhibition, Society for the Advancement of Material and Process Engineering, Longbeach, California (May 2004)*, 2004.

17 The Dow Chemical Company, *A Guide to Glycols (117-01682-0804XSI)*, 2003.

18 Fenn, A. J. and Shields, M. W., "Introduction to the New MIT Lincoln Laboratory Suite of Ranges," .

19 Richardson, R., Coyner, J., Fenn, A., and Brook, A., "Adaptive Techniques for Large Space Apertures," Tech. rep., Martin Marietta Aerospace Denver CO Denver Div, 1980.